Journal of Solid State Chemistry **149,** 349–353 (2000)
doi:10.1006/jssc.1999.8543, available online at http://www.idealibrary.com on IDEAL®

Redox Reaction of Praseodymium Oxide in the ZnO Sintered Ceramics

Naoki Wakiya, Sung-Yong Chun, Kazuo Shinozaki, and Nobuyasu Mizutani

Department of Metallurgy and Ceramics Science, Tokyo Institute of Technology, 2-12-1, O-okayama, Meguro-ku, Tokyo 152-8552, Japan

Received June 15, 1999; in revised form September 23, 1999; accepted October 22, 1999

The reason why Pr_2O_3 remains stable in the ZnO sintered body in air through pure Pr_2O_3 is only stable at high temperature was investigated using high-temperature XRD and thermogravimetry. The Pr_2O_3 in the ZnO sintered body was not due to reduction by the metallic Zn in the intestitial site of ZnO as reported in the literature. The redox reaction of praseodymium oxide in the ZnO grains is strongly affected by the microstructure. The reduction temperature of PrO_x with defect fluorite structure upon heating is increased with the decrease of PrO_x composition due to the decrease of open pores. On cooling, the oxidation of Pr_2O_3 into PrO_x is kinetically suppressed by the O_2 diffusion. In this way, Pr_2O_3 remains stable in ZnO sintered ceramics. © 2000 Academic Press

***Key Words*: ZnO; praseodymium oxide; high-temperature XRD; thermogravimetry; diffusion control.**

1. INTRODUCTION

A series of praseodymium oxide with general formula, Pr_nO_{2n-2} ($n = 4$, 5–6, 7, 9, 10, 11, 12) have been reported. (1–10). Among these compounds, Pr_2O_3 ($n = 4$) has both *A*- and *C*-type rare earth structure that are stable at high and low temperatures, respectively. Other compounds have a defect fluorite structure. In the following, the compounds having a defect fluorite structure are designated as PrO_x. Pure *A*-Pr_2O_3 is only stable at high temperatures above 1147 and 1376°C in N_2 and O_2, respectively (11). The *A*-Pr_2O_3 formed at high temperature is gradually oxidized in air into PrO_x as the temperature is lowered to room temperature (12).

Praseodymium oxide-added ZnO ceramics is a host material for varistor application (13–18). Since no compounds or solid solution occur in the ZnO–praseodymium system as shown in Fig. 1 (19), praseodymium oxide added in ZnO segregates at the grain boundary of ZnO ceramics and helps to form double Shottky barriers which is thought to be the origin of varistor characteristics along with other additives such as cobalt oxide. It has been reported that the redox states at the grain boundaries are very important for the double Shottky barriers (20–23). As mentioned above, Pr_2O_3 is not stable in air at room temperature; however, it has been reported that Pr_2O_3 in the ZnO ceramics remains stable without oxidation, even in air at room temperature. Since the redox states at the grain boundaries are very important, understanding the reason for the reduction of praseodymium oxide is needed. The literature described that the metallic Zn in the interstitial site of ZnO reduced PrO_x to Pr_2O_3 as in the following equation (12, 24):

$$n\mathrm{Zn(interstitial)} + 2\mathrm{PrO}_x \leftrightarrow n\mathrm{ZnO} + \mathrm{Pr_2O_3} + \left(X - \frac{n-3}{2}\right)\mathrm{O_2}. \qquad [1]$$

In the literature, the amount of PrO_x added into ZnO to fabricate a ZnO varistor is normally 0.5 mol% (24) with cobalt oxide. In this work cobalt oxide was not added for simplification of the redox reaction between ZnO and praseodymium oxide. We have already confirmed that Pr_2O_3 also remains stable in 0.5 mol% PrOX-added ZnO sintered body (25). To complete Eq. [1] in the sintered body, at least 0.25 mol% of interstitial Zn is required under the assumption that all interstitial Zn s segregated at the interface of PrO_x. However, the amount of n in the $Zn_{1+n}O$ has been reported to be 0.0003 (26), which is much smaller. Therefore, from the point of mass balance, the explanation using Eq. [1] is impossible. The target of this work is to clarify the reason why Pr_2O_3 remains stable in the ZnO sintered body.

2. EXPERIMENTAL

ZnO (99.9%, High Purity Chemicals, Japan) and Pr_6O_{11} ($PrO_{1.833}$) (99.9%, High Purity Chemicals, Japan) were used as starting materials. Powder having $y\mathrm{PrO}_x$–$(1-y)$ZnO composition was mixed with ethanol using a plastic jar and ZrO_2 balls for 24 h and dried using a rotary evaporator. For Pure ZnO and PrO_x, the powders of raw material were also milled by the ball milling under the same conditions (to compare the thermogravimetry (TG) profiles. The TG measurements were carried out using powder samples. The powders were loaded in a platinum crucible

0022-4596/00 $35.00

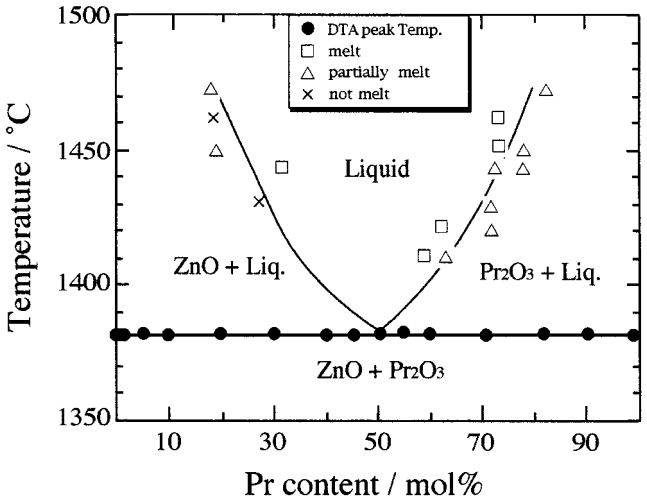

FIG. 1. The pseudo-binary-phase diagram in the Pr_2O_3 –ZnO system (19).

(1 ml in volume). The temperature was raised linearly from room temperature to1520°C (6°C/min) in air. For the correction of buoyant force, Al_2O_3 powder with the some volume of the sample was used. High-temperature powder X-ray diffraction (HTXRD) was measured from room temperature to 1400°C under N_2 and O_2 atmosphere. A small amount of powders was mixed with ethanol and the slurry was coated on the platinum plate. The platinum plate works as a heater for HTXRD by direct current carrying. The sample was heated at a heating rate of 10°C/min up to 700°C and kept for 5 min, and powder diffraction measurement were carried out between 20° and 50° 2θ at the scanning speed of 2° 2θ/min. The powder diffraction measurements were repeated at every 100°C (or 50°C) up to 1400°C. For each step, the heating rate was 10°C/min up to the prescribed temperature and kept so for 5 min before measurement. Detailed descriptions for the TG and HTXRD measurements were referred to in our previous work (11).

3. RESULTS AND DISCUSSION

Figures 2a and 2b show changes of the XRD intensity with temperature for pure $PrO_{1.833}$ and the powder mixture having $10PrO_{1.833}$–90ZnO composition when the samples were heated in N_2. In this figures, PrO_x, A-Pr_2O_3, and C-Pr_2O_3 denote a defect fluorite structure, A-, and C-type rare earth Pr_2O_3, respectively. These figures show that C-Pr_2O_3 forms between the temperature range 700–1000°C before formation of A-Pr_2O_3. The A-Pr_2O_3 formation temperature for pure $PrO_{1.833}$ and $10PrO_{1.833}$–90ZnO is almost the same (900°C) in N_2. The sudden decrease of the intensity of the ZnO (101) peak is due to the evaporation of ZnO on the measurement since the small amount of the slurry of the powder mixture was coated on a platinum heater. Figures 3a and 3b indicate the changes in the XRD intensity with temperature for pure $PrO_{1.833}$ and the powder mixture having $10PrO_{1.833}$–90ZnO composition in O_2, respectively. The A-Pr_2O_3 formation temperature for pure $PrO_{1.833}$ was 1400°C; on the other hand, that for $10PrO_{1.833}$–90ZnO was 1350°C. In an O_2 atmosphere, the formation of a trace of an unknown phase which was close to monoclinic Pr_2O_3 (ICDD card number: 22–880) (27) was also observed for $10PrO_{1.833}$–90ZnO between 1100 and 1300°C. The unknown phase was not detected for the pure $PrO_{1.833}$ sample. This fact indicates that the lowering of the Pr_2O_3 formation temperature occurred in a ZnO matrix in an O_2 atmosphere. It should be noted that the Pr_2O_3 formation temperature is an intensive variable. Therefore, the lowering of the Pr_2O_3 formation temperature in ZnO is evidence that ZnO behaves as a reducing agent of PrO_x into Pr_2O_3, even under the activity of oxygen which is equal to

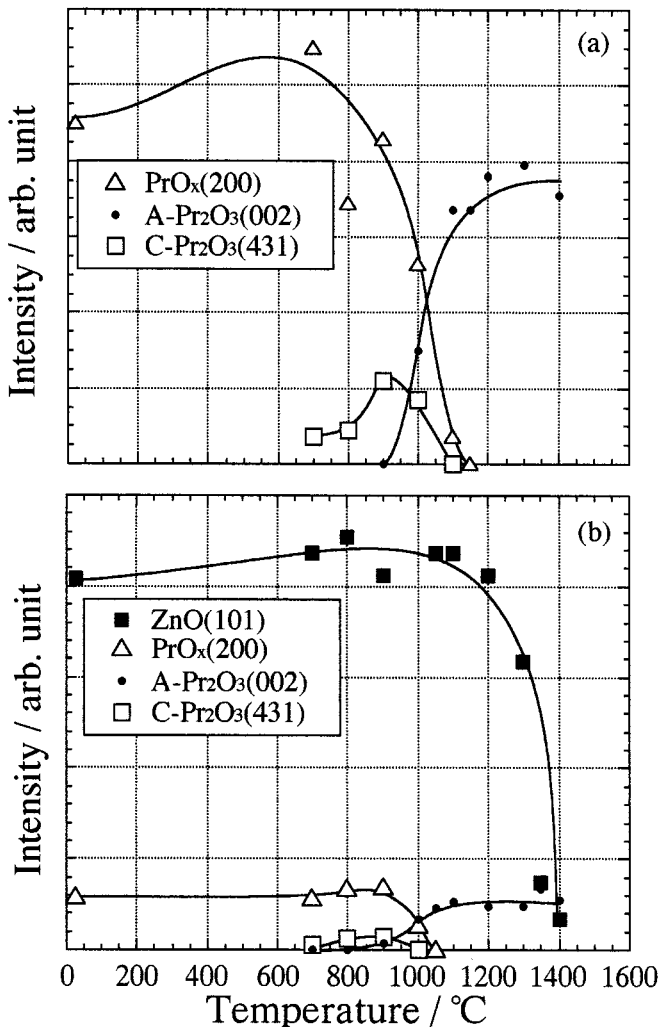

FIG. 2. Changes in the XRD intensity with temperature for (a) pure $PrO_{1.833}$ and (b) $10PrO_{1.833}$–90ZnO in N_2.

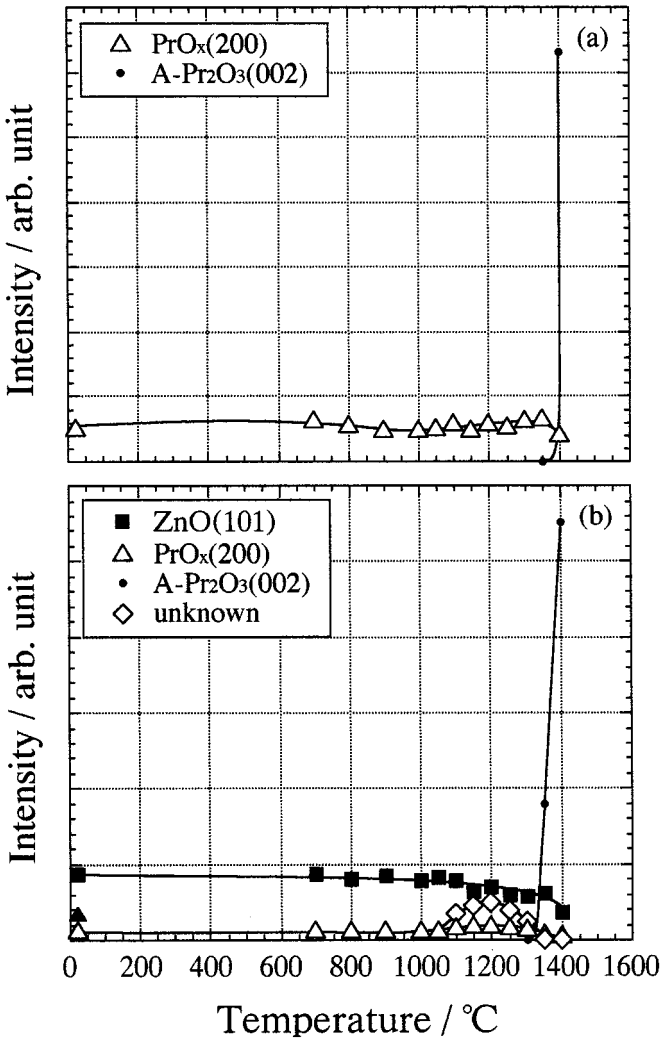

FIG. 3. Changes in the XRD intensity with temperature for (a) pure $PrO_{1.833}$ and (b) $10PrO_{1.833}$–90ZnO in O_2.

unity (O_2, 1 atm). This suggests that the reaction such as that shown in Eq. [1] would actually occur at the interface of the contacting points between ZnO and PrO_x grains as shown in Fig. 4; however, as mentioned above, it is impossible to apply Eq. [1] simply from the point of mass balance.

Figure 5 shows the changes of the weight for ① $PrO_{1.833}$, ② ZnO, and ③ $10PrO_{1.833}$–90ZnO with temperature in air. In this figure, the reported data by Hyde *et al.* (10) are also plotted for comparison. Their data were collected under 205 Torr oxygen pressure (the pressure was measured on a mercury manometer) and the heating rate was 1.5°C/min. Since our praseodymium oxide contained some adsorbed water, the weight change level of their data was − 1.8 wt% shifted to match the level of $PrO_{1.70}$ for our data an their data. Comparing to the two sets of data, it can be mentioned that the shape of the weight change–temperature curve is almost the same; however, the temperature of the reduction reac-

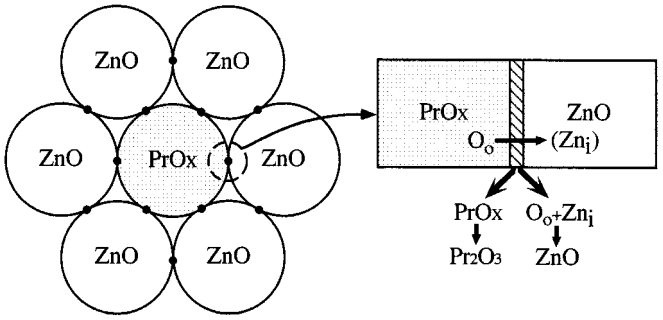

FIG. 4. Schematic redox reaction at the interface of the contacting points between ZnO and PrO_x grains.

tion was somewhat different. This would suggest that our measurement is partly kinetic due to the difference in the heating rate (6°C/min for us and 1.5°C/min for Ref. (10)). The heating atmosphere also affects kinetics. Their sample was heated in pure oxygen under reduced pressure; on the other hand, our sample was heated in air (oxygen partial pressure was around 152 Torr). This means that our sample was surrounded by N_2 gas having partial pressure of 608 Torr. Therefore, the dissociation speed of oxygen from the sample would be suppressed by the N_2 which would increase the weight change–temperature. In any case, the step-by-step weight loss of $PrO_{1.833}$ corresponds to the

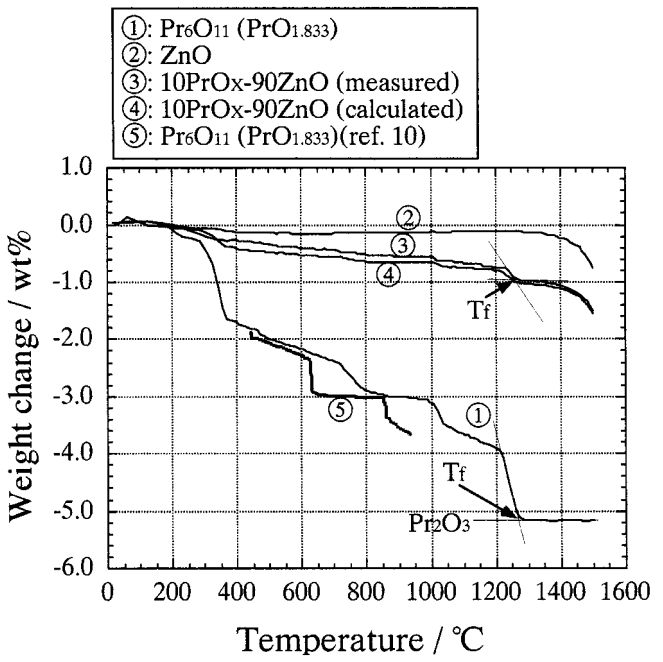

FIG. 5. Changes in the weight for ① pure $PrO_{1.833}$, ② pure ZnO, ③ $10PrO_{1.833}$–90ZnO (measured), and ④ $10PrO_{1.833}$–90ZnO (on the basis of ① and ② in air. ⑤ Reported data for $PrO_{1.833}$ measured under nominal oxygen pressure of 205 Torr (10).

changes of the phases until it reaches Pr_2O_3 (11). With the increase of the temperature, the curve becomes plateau, which has brought about the complete reduction of PrO_x into Pr_2O_3. In this work, the temperature is defined as T_f, which was determined by the crossing point of the tangential lines before and after the inflection point as shown in curve ①. Curve ② shows that significant weight loss due to the evaporation of ZnO occurs above around 1300°C. It is rather difficult to determine the T_f for $10PrO_{1.833}$–90ZnO because the data include the effect of the evaporation of ZnO. In Fig. 5, the calculated $10PrO_{1.833}$–90ZnO curve on the basis of the curves of pure $PrO_{1.833}$ and ZnO was also shown ④. By the comparison of curve ③ with ④, it can be mentioned that the measured $10PrO_{1.833}$–90ZnO curve is close to the calculated one; therefore, by the comparison, it was possible to determined the T_f for the mixture sample such as $10PrO_{1.833}$–90ZnO. By a careful observation, it was found that measured T_f is slightly different from the calculated one. Figure 6 shows the change of T_f with Pr content. This figure shows that T_f decreases with the increase of the Pr content and T_f in pure $PrO_{1.833}$ is lower than the mixture of $PrO_{1.833}$ and ZnO. It should be noted that the temperature at which the reduction of PrO_x into Pr_2O_3 is finished (T_f) is an extensive variable. If the reduction of PrO_x occurred at the interface of the contacting point between ZnO and PrO_x, T_f of PrO_x–ZnO should be lower than that of pure PrO_x; however, the result shown in Fig. 6 is contrary. This suggests that another mechanism should be considered. In Fig. 6, the relationship between the average grain size and PrO_x content after sintering took place at 1350°C for 2 h in air was also plotted. The average grain size was measured on the polished surface of the

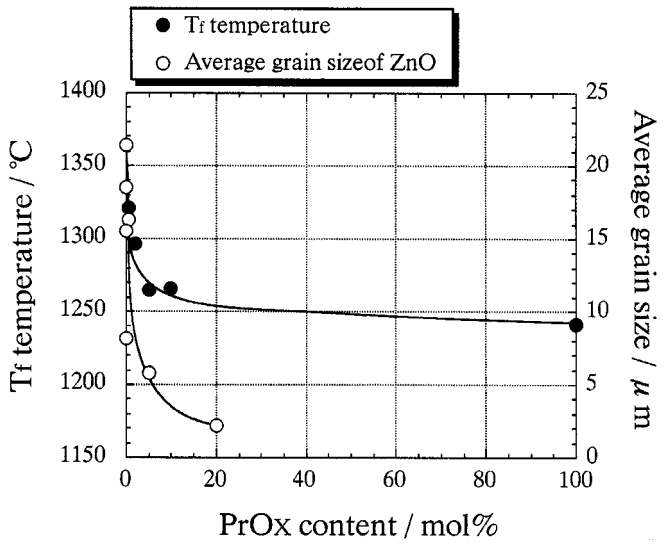

FIG. 6. Changes in T_f temperature with PrO_x content. The relationship between the average grain size and Pr content after the sintering at 1350°C for 2 h in air was also plotted.

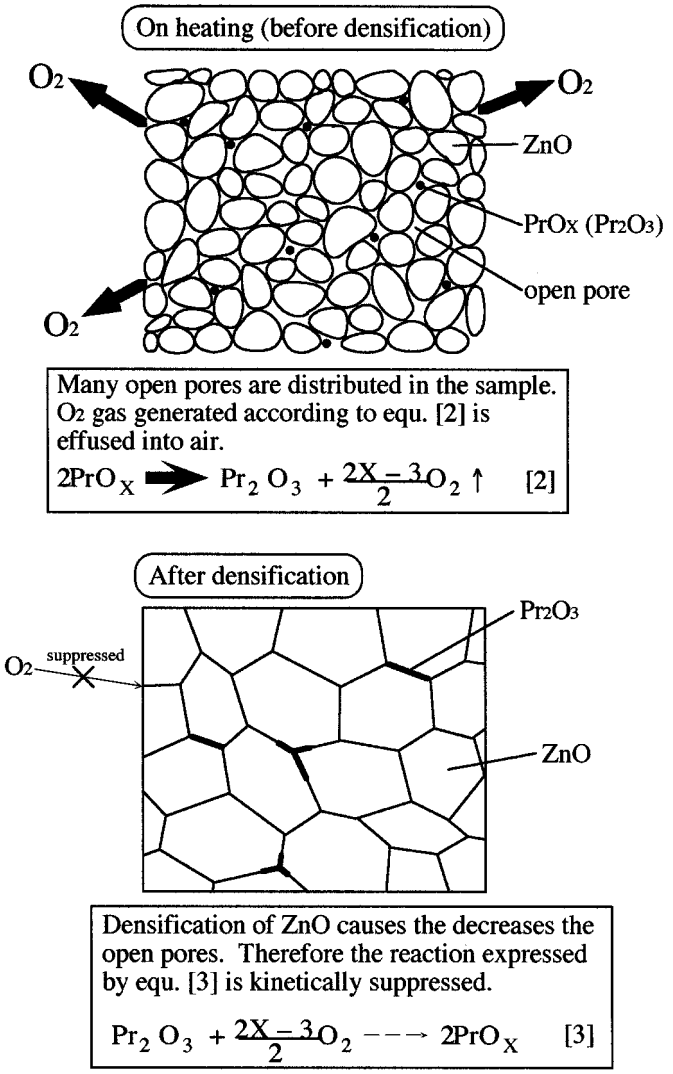

FIG. 7. Schematic model for the reason of remaining Pr_2O_3 in the ZnO ceramics.

sintered body using the linear intercept method. This figure shows that the grain size decreases with PrO_x content and the amount of segregation between ZnO grains increases with PrO_x content since no solid solution or compounds occur in the PrO_x–ZnO system. Therefore, before densification, the O_2 gas generated according to Eq. [2] effused into air via the opening of the ZnO grains since the grain boundary of ZnO is not formed as schematically shown in Fig. 7. Therefore, the result shown in Fig. 6 indicates that the dissociation of oxygen from praseodymium oxide is kinetically controlled, especially in the mixture of ZnO.

$$2PrO_x \rightarrow Pr_2O_3 + \frac{2X-3}{2}O_2\uparrow. \qquad [2]$$

Since the increase of the PrO_x content brings about the increase of open-pore density and a decrease of relative

density (11), the O_2 partial pressure at the inside part of the sample would not be increased due to the effusion of the O_2 gas generated according to Eq. [2]. On the other hand, for the sample with a small amount of PrO_x composition, the amount of open pores are decreased and the amount of closed pores is increased. Therefore, O_2 gas generated according to Eq. [2] cannot be effused, which causes the increase of oxygen partial pressure at the inside part of the sample. Therefore, the reaction expressed as in Eq. [2] is suppressed, which causes the increase of the T_f temperature.

If the redox reaction of Pr_2O_3 is controlled by thermodynamics, the reverse reaction of Eq. [2] would occur upon the cooling process. As reported previously (26), Pr_2O_3 exists only at the grain boundary and triple point of ZnO grains and no open pores are observed after sintering (25). Therefore, upon the cooling process, the reverse reaction of Eq. [2] would be kinetically suppressed due to the hindrance of O_2 diffusion as schematically shown in Fig. 7. Actually, the pellet having $10PrO_{1.833}$–90ZnO composition and being sintered at 1350°C for 2 h in air was ground into powder and the resultant phases were examined using high-temperature XRD. At room temperature, the resultant phase was PrO_x and Pr_2O_3 as praseodymium oxide. Then, the powder was heated in air at 600°C. As the result, Pr_2O_3 is oxidized into PrO_x. This result supports the fact that the oxidation reaction of Pr_2O_3 into PrO_x is kinetically suppressed.

4. CONCLUSIONS

In this work, a new mechanism for the remnant of Pr_2O_3 in PrO_x-added ZnO ceramics was proposed via the investigation of the redox reaction between praseodymium oxide and ZnO. Thermogravimetric analysis in air for the powder mixture of PrO_x and ZnO revealed that the temperature at which the reduction of PrO_x into Pr_2O_3 is completely finished (T_f) increased with the increase of the ZnO composition. The average grain size of ZnO is decreased by the increase of PrO_x content, which indicates that the amount of the grain boundary increases with PrO_x content. Since no solid solution or compounds occur in the PrO_x–ZnO system, added PrO_x segregates between the ZnO grains. Before densification, the O_2 gas generated by the dissociation of PrO_x effused into air via the opening of the ZnO grains. The decrease of PrO_x composition causes the decrease of open pores and increase of closed pores. Therefore, the oxygen partial pressure at the inside part of the sample is increased, which raises the T_f temperature. Upon the cooling process, the oxidation of Pr_2O_3 into PrO_x is kinetically suppressed by the hindrance of O_2 diffusion. In this way, Pr_2O_3 remains stable in the ZnO sintered ceramics.

ACKNOWLEDGMENTS

This work was supported by a Grant-in-Aid for Scientific Research from the Ministry of Education, Science and Culture (No. 09450242).

REFERENCES

1. E. Daniel Guth, J. R. Holden, N. C. Baenziger, and LeRoy Eyring, *J. Am. Chem. Soc.* **20,** 5239 (1954).
2. R.E. Ferguson, E. Daniel Guth, and L. Eyring, *J. Am. Chem. Soc.* **76,** 3890 (1954).
3. E. Alesin and R. Roy, *J. Am. Ceram. Soc.* **45,** 18 (1962).
4. D. A. Burnham and L. Eyring, *J. Phys. Chem.* **72,** 4415 (1968).
5. J. Kordis and L. Eyring, *J. Phys. Chem.* **72,** 2044 (1968).
6. J. Zhang, R. B. Von Dreele, and L. Eyring, *J. Solid State Chem.* **122,** 53 (1996).
7. L. G. Liu, *Earth Planetary Sci. Lett.* **49,** 166 (1980).
8. J. O. Sawyern, B. G. Hyde, and L. Eyring, *Bull. Soc. Chim. France* 1190 (1965).
9. S. Yao, H. Tanaka, and Z. Kozuka, *J. Jpn. Inst. Met.* **55,** 1216 (1991).
10. B. G. Hyde, D. J. M. Bevan, and L. E. Eyring, *Philos. Trans. R. Soc. London Ser. A* **259,** 583 (1966).
11. N. Wakiya, S. Y. Chun, A. Saiki, O. Sakurai, K. Shinozaki, and N. Mizutani, *Thermochim. Acta* **313,** 55 (1998).
12. Y. S. Lee, K. S. Liao, and T. Y. Tseng, *J. Am. Ceram. Soc.* **79,** 2379 (1996).
13. J. D. Levine, *CRC Crit. Rev. Solid State Sci.* **5,** 597 (1975).
14. K. Mukae, K. Tsuda, and I. Nagasawa, *Jpn. J. Appl. Phys.* **16,** 1361 (1977).
15. G. D. Mahan, L. M. Levinson, and H. R. Philipp, *J. Appl. Phys.* **50,** 2799 (1979).
16. G. Blatter, and F. Greuter, *Phys. Rev. B* **33,** 3952 (1986).
17. G. Blatter, and F. Greuter, *Phys. Rev. B* **34,** 8555 (1986).
18. M. Rossinelli, F. Greuter, and F. Schmuckle, *Br. Ceram. Proc.* **41,** 177 (1989).
19. S. Y. Chun, N. Wakiya, H. Funakubo, K. Shinozaki, and N. Mizutani, *J. Am. Ceram. Soc.* **80,** 995 (1997).
20. F. Greuter and G. Blatter, *Semicond. Sci. Technol.* **5,** 111 (1990).
21. G. Blatter and F. Greuter, *Phys. Rev. B* **33,** 3952 (1986).
22. J. Tanaka, H. Haneda, S. Hishita, A. Watanabe, C. Akita, N. Ohashi, and S. Tanaka, *Mater. Sci. Forum* **126–128,** 741 (1993).
23. S. Tanaka, C. Akita, N. Ohashi, J. Kawai, H. Haneda, and J. Tanaka, *J. Solid State Chem.* **105,** 36 (1993).
24. K. Mukae and I. Nagasawa, *Adv. Ceram.* **1,** 331 (1981).
25. M. Shida, S. Y. Chun, N. Wakiya, K. Shinozaki, and N. Mizutani, *J. Ceram. Soc. Jpn.* **104,** 44 (1996).
26. R. Wang and A. W. Sleight, *J. Solid State Chem.* **122,** 166 (1996).
27. Willer and Daire, *Bull.Soc. France Min. Crist.* **92,** 33 (1969).